Universidad Zaragoza
1542

Trabajo Fin de Máster

Fabricación y Testeo de Micropreconcentradores basados en Si modificados con materiales tipo MOF para Adsorción de Gas Sarin

Fabrication and Testing of Si based Micropreconcentratos modified with MOF type materials for Sarin Gas Adsorption

Autor/es

Jorge Fantova Sarasa

Director/es

María Pilar Pina Iritia
Miguel Ángel Urbiztondo Castro

Facultad de Ciencias

2017

List of abbreviations

MOF: Metal Organic Framework

PECVD: Plasma-enhanced chemical vapor deposition

SAM: Self-assembled monolayer

LbL: Layer by Layer

DMMP: Dimethyl methylphosphonate

MS: Mass spectrometer

SEM: Scanning electron microscopy

TGA: Thermogravimetric analysis

XRD: X-ray diffraction

SBU: Secondary building unit

RT: Room temperature

DMF: Dimethylformamide

DFT: Density functional theory

DI: Deionized

BET: Brunauer, Emmett and Teller

MHDA: 16-mercaptohexadecanoic acid

IDLH: Immediately dangerous to life and health

NPT: Normal pressure and temperature.

Table of Contents

1 Introduction

The discovery of chemical warfare agents (CWA) during the last century has provided global terrorism another particularly deadly weapon to inflict harm. Their danger is derived from their high toxicity, difficulty to be detected by the senses and its high persistency and rate of propagation. Among them there is the Sarin gas, which heavily affects the nerve system and can produce death within hours or even minutes of exposition. It is responsible for causing 5500 injured and 12 deaths in the attacks at Matsumoto city (1994) and the Tokyo subway system (1995) by a Japanese cult [1].

As these agents are inexpensive to manufacture and can be produced even by small terrorist groups, military forces present in highly conflicted areas must be prepared to detect CWA at concentrations far lower than the immediately dangerous to life and health (IDLH) value, which is 0.1 mg/m^3 [2] or around 17 ppb in the case of the Sarin gas at normal temperature and pressure (NTP) conditions.

One of the solutions proposed to deal with this issue is the concept of an "electronic nose", a portable device with the purpose of sensing these harmful vapors. One of the core apparatus of the electronic nose developed within the research group of this Master's thesis (Nanostructured Films and Nanoparticles) are the microcantilever platforms, which are able to detect a quantity of adsorbed material on top of them in the range of ng by evaluating its vibration frequency shift during the process, all in a lapse of few minutes.

The problematic of these devices are that merely sampling the atmosphere is not efficient, as their main components (nitrogen and water vapor) are injected as well, masking the signal of the compound desired to sense. On one hand, nitrogen represents an obstacle as the principal dilutant of the sample, as 79 vol.% of air is composed of it, meaning the potential sensitivity is haltered by the gas. On the other hand, the presence of water interferes with the activity of the sensing materials, as the molecules tend to adsorb into their micropores.

Because of these aspects, a desirable improvement for this equipment could be a "micropreconcentrator" (µPC), a compact and sealed device comprised of a plate grown with sensing material that selectively adsorbs volatile compounds and a heater to promote its desorption. After enough sample has been injected, the inlet is closed, the

air evacuated and the heater is switched on to desorb the vapor molecules, which can proceed into the microcantilever section, now in much higher concentration.

Having all this background in mind, the present work was focused in the fabrication of a functional µPC and its activation with a robust and hydrophobic microporous metal organic framework (MOF) type sensing material. The resulting microdevice was evaluated in the adsorption of dimethyl methyl phosphonate (DMMP) which is a well-known simulant of the Sarin gas, at ppm level in the gas phase. In addition, a comparison between the adsorption performance of the bulk MOF in a fixed bed reactor configuration and the thin layer of MOF grown on the surface of the Si based µPC was planned.

In particular, while the plate used for the growth of the MOF was Pyrex due to its affordability, the base material of the µPC was silicon due to its deep integration within the world of microelectromechanical systems (MEMS), which can yield benefits such as sharper desorption pulses and low energy cost [3].

The selected MOF was an analogue of the MOF-5 built from sublimated zinc acetate and a carboxypyrazole-terminated ligand, the so-called "Zn-DMCAPZ". The basis for its election was mainly its high hydrophobicity and thernal resistance. Apart from the growth of the MOF on top of the Pyrex plates, this material was also synthesized in powder form to determine its DMMP sorption isotherm and to prepare the fixed bed.

2 Microdevices, materials and methods

2.1 Si based micropreconcentrators

The fabrication process of the µPC involves a long sequence of microfabrication processes, starting at the photolithography process of the wafers and ending with the heater gold deposition at the back of the sealed device. Essentially, it can be divided into the channel definition of the silicon base, the lithography and growth of sensing material over the Pyrex cover, the evaporation of a backside heater and the sealing of both parts by high temperature resistant glue. The procedure followed in this work was replicated from [3], with a few exceptions, and was schematically illustrated in **¡Error! No se encuentra el origen de la referencia.**.

The starting material for the base were silicon wafers of 4 in. diameter (500±20 µm thick, following a <100> orientation, "p" doped with a resistivity of 5-10 Ω·cm

provided by Sil'Tronix Silicon Technologies. A layer of negative-working photosensitive resist ProTEK® PSB (Brewer Science) was applied prior to photolithography, whose main feature is its non-degradability upon wet etching by potassium hydroxide (KOH). After the photolithography has been carried out, the etching is performed by immersing the substrate in a 40% w/v solution of KOH at 80ºC for 1 h, which results in the definition of channel depth of around 100 µm. Following this operation, the removal of the photoresist (or "lift off") is executed by submerging the Si wafer in "piranha solution" (1:4 v/v of H_2O_2 30 $wt.\% : H_2SO_4$ 95$wt.\%$) subjected to an ultrasonic bath, after which it is cleaned with DI water while remaining in a sonic bath. The complete elimination of the resist is crucial to achieve a good sealing of the device. The final preparation steps for the Si wafer involves the photolithography of its back side; a deposition of 2 layers of 10 nm of Cr plus 150 nm of Au, in that order, by electron beam physical vapor deposition (EB-PVD) (Edwards auto-500) employing the photolithography resist TI35ES (Microchemicals) as a sacrificial layer and the lift-off of the metal layer by immersion in a sonicated bath with acetone, yielding a heater for the µPC.

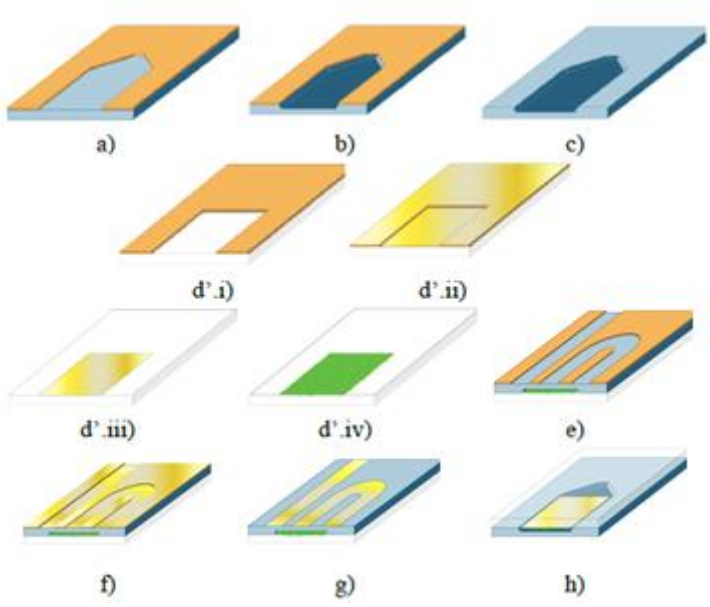

Fig. 1 General microfabrication scheme for microconcentrator with integrated MOF-5 layer. a) Photolithography process on Si wafer. b) Definition of the channel by KOH etching. c) Removal of the photoresist. d'.i) Photolithograpy process on Pyrex wafer. d'.ii) 10 nm of Cr and 50 nm of Au layer deposition on Pyrex wafer. d'.iii) Lift-off by acetone immersion. d'.iv) Growth of the MOF layer on separated Pyrex substrates (LbL). e) Photolithography on the backside of the Si wafer. f) Au layer deposition on the backside of Si wafer. g) Lift-off on the backside. h) Sealing by application of glue. Image extracted from [4].

As stated before, the cover for the µPC was Pyrex, which also suffered a photolithography step to define the feature desired to achieve. Then, 2 layers of Cr and Au of 10 and 50 nm, respectively, were evaporated in that order on top of the Pyrex by the same procedure that the used in the case of the heater. At this point, the growth of the Zn-DMCAPZ over the Pyrex layer is carried out. The bonding of the Si base and the Pyrex cover is performed by gluing both parts with Acc Silicoset 158, which endures up to 300 ºC.

Lastly, for the connection of the µPC to the transfer lines, 1 mm diameter ports were drilled on the Pyrex side by sand blasting process (Alumina dust 170 mesh). Fused silica capillaries (0.32 mm internal diameter) were connected to the µPC by means of silicone septum glued on the Pyrex port (see **¡Error! No se encuentra el origen de la referencia.**). Finally, quartz adapters were used for the capillaries' junctions.

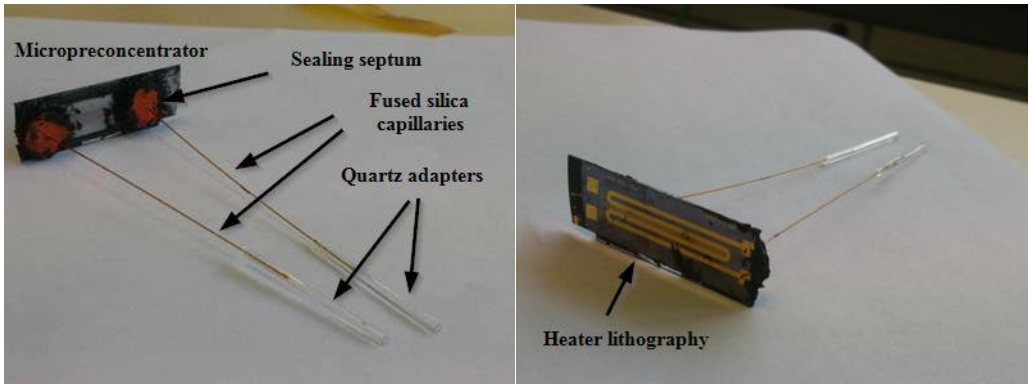

Fig. 2 Front and backside view of the fabricated µPC.

The photolithography mask design for both the Si and the Pyrex plates can be found at **¡Error! No se encuentra el origen de la referencia.**, and the pattern corresponding to the heater along with the final view of the silicon substrate prior to the Pyrex bonding at **¡Error! No se encuentra el origen de la referencia.**.

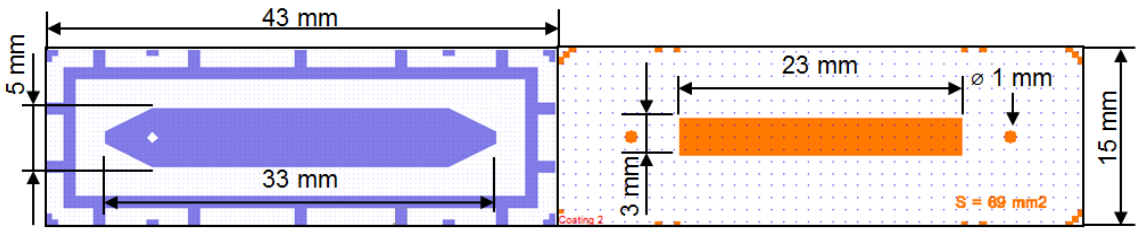

Fig. 3 Mask design for the patterning of: the top Si surface (left) and the top Pyrex surface (right). The color blue corresponds to the area exposed to the Si anisotropic etching and the orange to the area exposed to Cr and Au e-beam PVD.

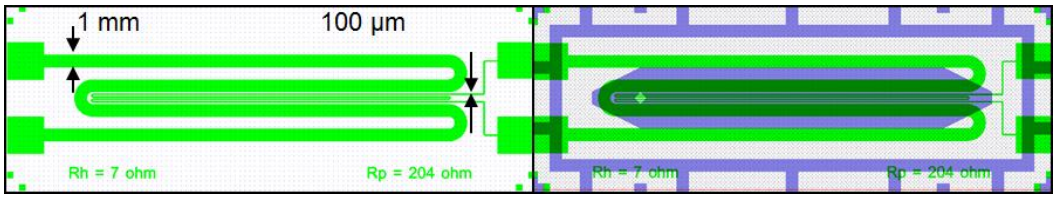

Fig. 4 Mask design for the patterning of the Cr-Au heater on the back Si surface: the color green corresponds to the area exposed to Cr and Au e-beam PVD(left) top view of the final Si plate before bonding to the Pyrex cover (right).

2.2 MOF-5 analogue: Zn-DMCAPZ

As any other MOF material, Zn-DMCAPZ is composed of an arrangement of metal-based agents and organic ligand building blocks. For this variation in particular, the first compound was the zinc acetate cluster $Zn_4O(OAc)_6$, and the second was 3,5-Dimethyl-4-carboxypyrazole ($H_2dmcapz$ 97% from Sigma-Aldrich). All the information regarding the characteristics and synthesis procedures for both the bulk powder and the layer growing was extracted from the dissertation of Angelique Bétard from the Ruhr University Bochum [5].

While the ligand employed was of commercial quality, the "basic" acetate was synthetized from zinc acetate dihydrate ($Zn(AcO)_2 \cdot 2H_2O$ 99.99% trace metal basis from Sigma-Aldrich). The hydrated acetate was loaded into a schlenk and heated up to 280 ºC under vacuum in a sand bath. In the following 2 hours the white crystals sublimated around the walls of the schlenk, which was cooled by a water tap coil. After harvesting and milling the crystals, the yield of the process was of approximately 62%.

Once both the metal and the ligand compounds were available, several batches of Zn-DMCAPZ were produced following the so-called "secondary building unit (SBU) approach". First, a solution of basic zinc acetate in 1:1 v/v ethanol:dimethylformamide (DMF) was mixed with a solution of ligand in 3:1 v/v ethanol:water, ensuring a molar proportion of ligand/basic acetate equal to 3 and taking a basis of 500 mg of ligand. After mixing at room temperature (RT), a sudden precipitation of white crystal occurs. The solution is put in an over at 50 ºC for 1 h to allow full crystallization and is then stored overnight at RT. Then, the supernatant is discarded and the remaining crystals are collected by centrifugation, then subsequently washed and centrifuged in deionized (DI) water, ethanol and ether. The final step involves the activation of the powder, i.e removal of solvent traces, by heating in a vacuum oven at 110 ºC for 3 days to ensure

the complete removal of all remaining solvents within the solid, yielding the desired Zn-DMCAPZ in powder form with the majority of its crystals below 200 nm diameter.

2.3 In situ Growth of Zn-DMCAPZ layers on the µPC

The method employed to grow the Zn-DMCAPZ material on top of the Au coated Pyrex plates was the so-called layer by layer (LbL) and was adapted from [5], as in this case a Pyrex substrate was employed instead of alumina or silicon substrate. It is based in separating the metal cluster or SBU ($Zn_4O(OAc)_6$) of the MOF from the organic linker ($H_2dmcapz$) in 2 different solutions and immersing the substrate subsequently in both solutions. Between each step, a submersion of the substrate in pure ethanol is required to remove the excess and those species loosely attached to the substrate.

The first step was the surface cleaning by subsequent immersion in isopropanol, acetone and DI water. Then, the samples were treated with oxygen plasma employing a SISTEC 600 plasma-enhanced chemical vapor deposition (PECVD) equipment, in order to eliminate all remaining organics and to expose hydrophilic reactive groups on its surface.

The optimal set of parameters established were the "Plasma 2", which can be found at the paragraph down below along with its less effective condition setup:

- "Plasma 1": Power of 300 W, pressure of 0.19 mbar, oxygen flux of 20 sscm, all during a time lapse of 30 min.
- "Plasma 2": Power of 200 W, pressure of 0.4 mbar, oxygen flux of 50 sscm, temperature of 120 ºC, bias voltage of 22 V, all during a time lapse of 30 min.

The last step before the LbL is the modification of the surface's activity by the formation of carboxylic acid self-assembled monolayers (SAMs). Thus, the plates were immersed right after the plasma treatment in a 20 µM 16-mercaptohexadecanoic acid (MHDA 99% from Sigma-Aldrich) solution with 95:5 v/v ethanol:acetic acid volumetric proportion, where they were incubated for 24 h. After this process, the plates were washed in a 90:10 v/v ethanol:acetic acid solution and dried by an air stream. The method is based on the affinity between the gold surface of the substrate and the thiol reactive group of the MHDA, leaving the carboxylic group exposed on the surface in order to promote the LbL assembly.

Following the activation process, the MOF growing by LbL is carried out using the solutions described below:

- The metal-based solution was 1 mM in $Zn_4O(OAc)_6$ dissolved in 1:1 v/v ethanol:DMF, taking 80 mL as total volume basis.
- The linker-based solution was 0.5 mM in $H_2dmcapz$ dissolved in 3:1 v/v ethanol:DI water, taking 80 mL as total volume basis.
- The cleaning solutions contained 80 mL of pure ethanol (absolute grade).

Each solution was placed in a 100 mL glass beaker and immersed in the same oil bath at 50 ºC subjected to magnetic stirring and the duration of each immersion step was of 5 minutes. It is worth noting that the metal and linker solutions were only stirred until their respective powders were fully dissolved. After the desired number of LbL cycles had been achieved, the plates were simply dried in an air stream. A scheme of the procedure is found at Fig. 5.

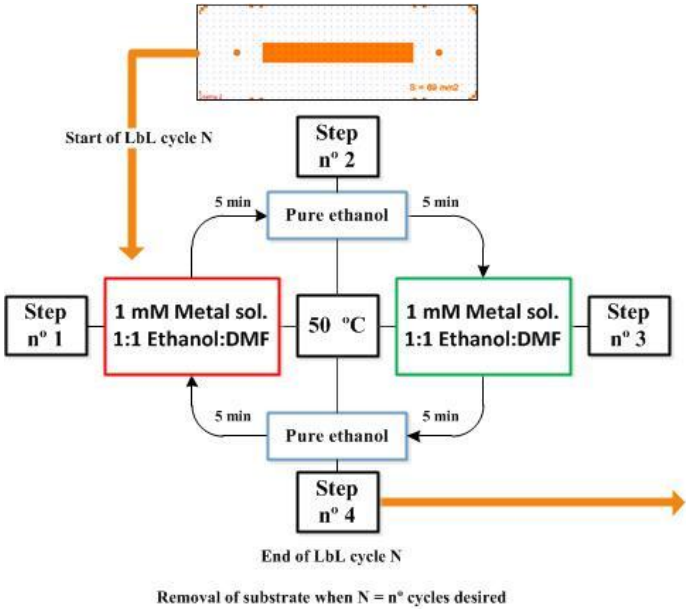

Fig. 5 Scheme of the sequential LbL process.

2.4 DMMP Sorption Performance Evaluation

2.4.1 Determination of the Adsorption Isotherm for DMMP vapors by TGA

In order to calculate the equilibrium for the DMMP adsorption of the MOF-5 analogue, sample of the sensing material was loaded into a quartz tube in an oven maintaining the set point of 30 ºC for the following supply of a DMMP flow of different concentrations via 2 saturators, which were modified by altering the temperature of the oil bath (5, 10, 15, 20 and 30 ºC) containing them.

When first introduced into the oven, the MOF sample undergoes a purification process by supplying a stream of 80 mL/min of dry nitrogen at 200 ºC for 24h. After

this step, a DMMP current of 80 mL/min courses through the material for 12 hours. Then, a sample of the material is carried to the TGA for its desorption, deducing by the difference of weights the total adsorbed mass of DMMP. An average of 4 samples was taken for each condition with a time lapse of 4h between them. The desorption analysis was performed under nitrogen atmosphere and with a temperature range of 30 – 350 ºC, with a heating rate of 5 ºC/min. The relative pressure of DMMP (P) was estimated by the Law of Antoine, solving the equation with the input of the temperature of the saturators' oil bath. The process was repeated a minimum of 4 times for each set of conditions.

The data collected from this experience was fitted to the Langmuir-Freundlich equation and plotted along with its characteristic parameters in Fig. 6.

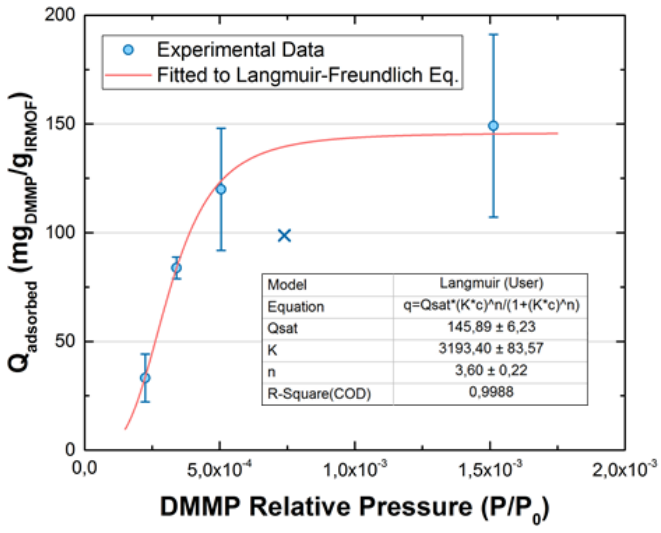

Fig. 6 Langmuir adsorption isotherm of Zn-DMCAPZ for DMMP at 30 ºC

2.4.2 Standard Characterization of Micropreconcentrators

Generally, the dynamic retention capacity of a micropreconcentrator is measured by monitoring a constant draw of sample through the device. An important time mark is $t_{0.10}$, which is the time at which the concentration of the sample has achieved 10 % of its maximum value ($C = 0.10*C_0$), in other words, the breakthrough time. Typically, the adsorption of every µPC experiment is paired with the complementary test of a blank µPC (non-grown material). This is done as, ideally, the inclusion of a sensing material in the µPC means that in the first minutes the adsorbate will not be shown on the detector as it is being trapped within the material, thus the existence of a delay time.

(Fig. 7) shows this effect, as there are approximately 42 minutes of delay in between the breakthrough of the blank curve and that of the adsorbing material [6].

The saturation point is also critical in the characterization of the µPC, and it is defined as the time required to visualize 95% of the maximum adsorption value (C = 0.95* C_0). It is from this point on that the stream tunneling through the µPC would shift to pure dry nitrogen and the heater integrated within the device would be switched on if the desorption was to be measured.

The contrast of these 2 points yield the so-called sorption efficiency of the µPC, which is one of the main parameters of said device that allow its standard comparison to that of other works. This value is calculated by dividing the useful capacity of the µPC q_e by its real capacity q_s, which, taking Fig. 7. left as a reference basis, would take the fraction of the labeled areas A and B:

$$sorption\ efficiency = \frac{q_e}{q_s} = \frac{A}{A+B}$$

In addition, to measure the raw adsorption capability of a material one must consider that in absence of sensing agent all the concentration of the gas is that of the maximum of the equilibrium at the initial time t_0. Then, by subtraction of real area under the adsorption curve (D) from the hypothetical maximum adsorption at t_0 one discovers the area directly related to the adsorbed mass by the material (C). Such operation was to be applied to the results of the kinetic adsorption experiments of the fixed bed reactor and the µPC. Fig. 7. right illustrates the area regions mentioned before (C, D).

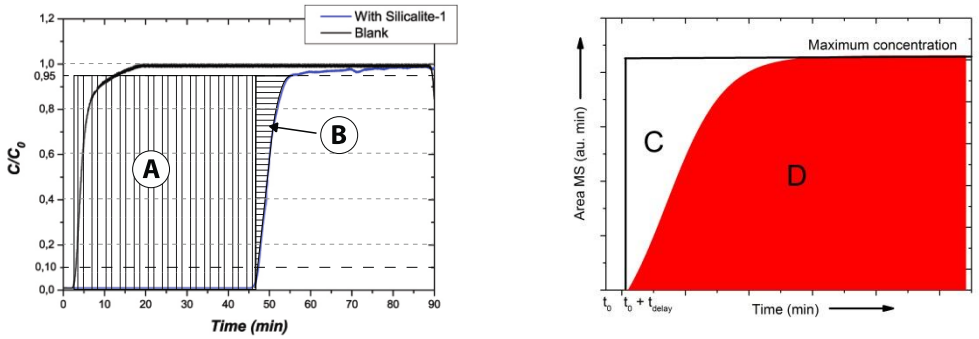

Fig. 7 Comparison of the Break-through curve for type A design without (blank) and with silicalite-1 layer. Image extracted from [6] (left); indication of the area related to the mass adsorbed in a kinetic experiment (C).

2.4.3 Experimental Set up

Throughout the course of the experiments, multiple configurations of the plant were tested depending of the substance analyzed and the property of study, and can be classified under hexane analysis setup (Fig. 8), injection setup (Fig. 9) and adsorption setup (Fig. 10).

The sample loop employed in all cases had a volume of 1.8 mL and it was used as a means of discretizing the sample into pulses of known concentration (as in **¡Error! No se encuentra el origen de la referencia.**), as the analysis of a continuous stream of DMMP might not be feasible due to its long lasting time within the transfer lines. It is worth noting that for all the experiments involving DMMP, the pipe lines in between the source of DMMP and the beginning of the MS had to be heat insulated (as in Fig. 9), as the boiling point of that substance is 181 ºC and, were it not insulated, it would get stuck all along the pipe lines, thus yielding false readings of concentration. The heating tapes had a power of 250 W/m and the estimated temperature achieved within the pipes was of approximately 140 ºC.

The source of hexane for all its experiments was a synthetic mixture from a certified gas cylinder containing 500 ppmV of n-C_6H_{14} in dry N_2 (purchased from Air Products and Chemical. Inc.). However, the stream was diluted with dry N_2 (99.999%) by means of mass-flow controllers until the 100 ppmV, which were consistently pumped into the loop at 80 mL/min. The altered variable was the flux of the carrier gas (nitrogen) from 5 to 100 mL/min and 3 loop pulses were registered under each condition. The reason behind the tests was to discover the hexane signal processing parameters of the MS, such as the delay or recovery time of said signal.

As stated before, the character of DMMP does not allow for continuous monitoring of the substance, especially in the kinetic adsorption experiments. Thus, the strategy to measure the evolution of the process was to install a setup similar to that of [7], whose strategy is to continuously draw the adsorbate (DMMP in this case) through the µPC and into a loop, homogenizing the line. Then, switching the valve, a stream of dry nitrogen sweeps the loop and carries the signal to the MS, obtaining the concentration present in the micropreconcentrator at the time of switching of the valve, approximately. In this manner, periodical switches of increasing timing lapses in between them (from 1 up to 10 min) were done to define the kinetic adsorption curve for either the fixed bed reactor or the µPC. The scheme of the plant is found at (Fig. 10).

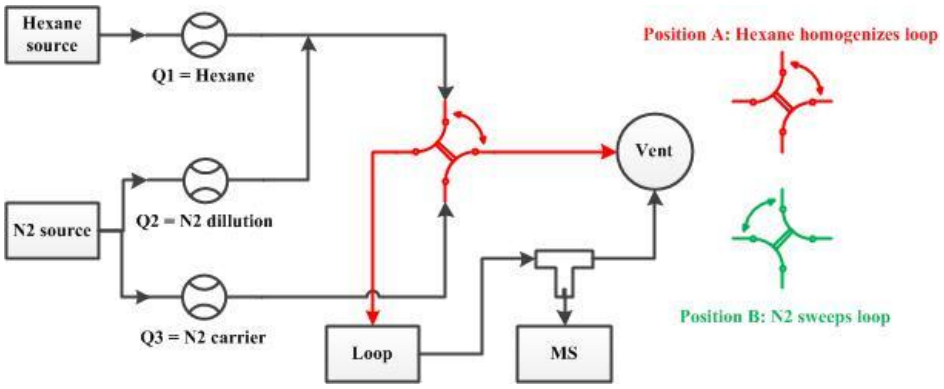

Fig. 8 Scheme of the plant used to measure hexane.

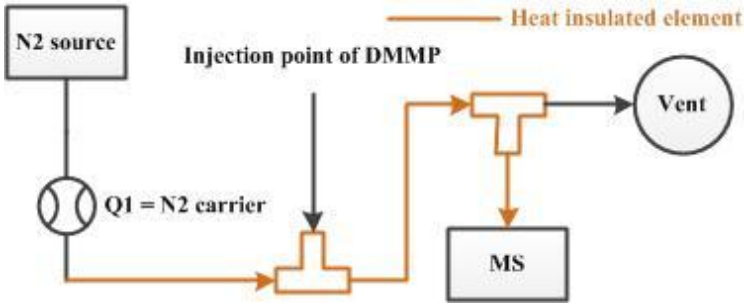

Fig. 9 Scheme of the plant employed to calibrate the MS to DMMP injections.

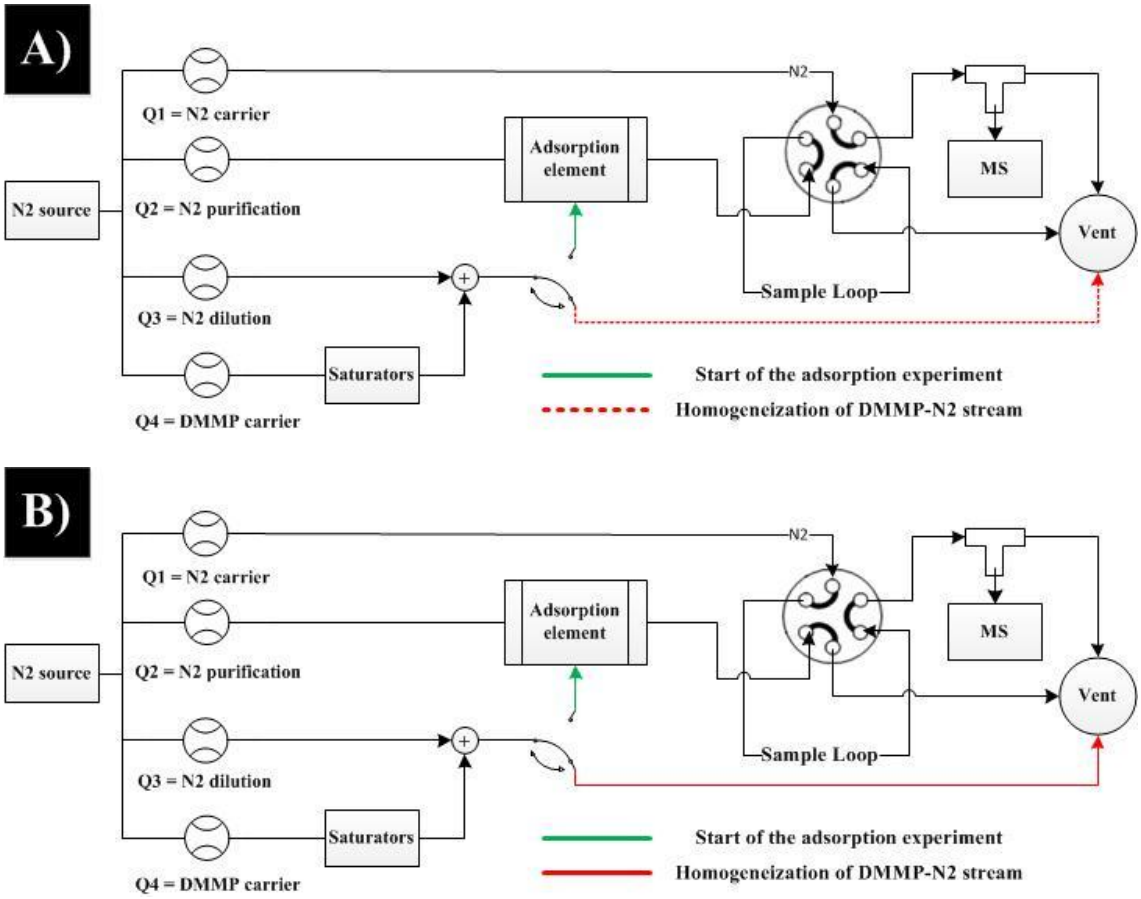

Fig. 10 A) Configuration to homogenize the sample loop with DMMP-N2 stream. B) Configuration to sweep the loop and carry its signal to the MS. Scheme inspired from the supplementary information of [7].

2.4.4 Calibration of Mass Spectrometer for DMMP vapors

An Omnistar GSD301O2 Mass Spectrometer (Pfeiffer Vacuum) was used on line to monitor the DMMP concentration in the gas streams.

In the case of DMMP, its main corresponding peaks are, in descending order: 94, 79 and 109 uma. Nitrogen and hexane were also analyzed in the work and their respective representative peaks were 28 and 57 uma. The analysis of hexane was performed at the beginning of the MS experiments in order to contrast the behavior of DMMP in terms of delay and recovery times as well as its persistency in the system. Also, unlike stated otherwise the flow rate for all the gases in the plant was of 80 mL/min.

In order to perform the right analysis of the DMMP signal by MS, the first stage of the experiments was devoted to understanding its response and the effect of the various parameters set for the measurement, such as dwell time or resolution of the signal.

Apart from a first determination of the true main peak (94 uma) corresponding to DMMP, which was the same as the reported by the literature, a screening of different resolution and dwell time values was performed. The first parameter is related with the tolerance of the program to relate a signal with a value of uma, in other words: higher resolution signifies the acquisition of broader peaks for the same uma value. The other property indicates the amount of time the MS detector will consume acquiring data and displaying an output. While higher values of dwell time provide signal of less noise, the frequency of signal collection is reduced, which could be a nuisance when trying to collect the data of a very narrow and fast pulse, as it may achieve its maximum concentration in between measurements. Fig. 11 represents the change of the DMMP signal when adjusting both values, whose influence is slightly present in the overall height of the peaks and noise of the signal when shifting resolution. However, the hypothesis stated previously was realized for the dwell time. With this information, the parameters selected for the rest of the experiments were a dwell time of 200 ms, resolution of 50 and carrier flow of 80 mL/min.

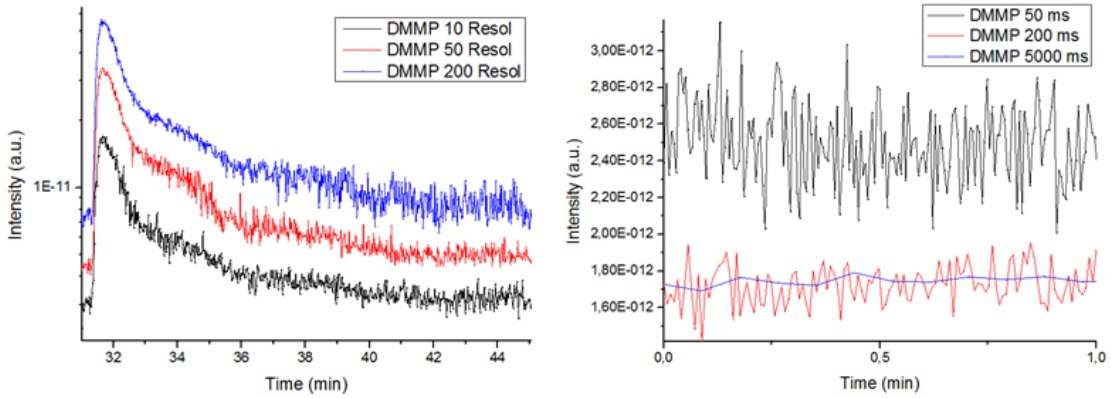

Fig. 11 Comparison of DMMP's MS signal (94 uma) processing by changing the resolution parameter (left) and dwell time (right).

The MS calibration pursues to establish a relation between a known amount of DMMP introduced to the MS and the value of integral under the curve corresponding to that mass. One option could have been sampling with a pair of saturators assuming that they achieved the DMMP saturation point at a certain temperature, but it was initially discarded due to the suspected low efficiency of the saturators.

The first setup attempted for the DMM calibration is shown at Fig. 9. It mainly consisted of heating tapes of 250 W/m, and pure DMMP in liquid phase was injected with a syringe of 100 microliters. While the signal collected was huge (shown in Fig. 12, left), its drawbacks were a long lapse of time necessary to clean the transfer lines of DMMP and the limitation of concentration, which was far beyond the 100 ppm value.

As the main problem was the high concentration of the compound, injection of DMMP with a diluting agent was studied. Several substances were employed such as isopropanol and chloroform, mainly. Starting from a mother solution of DMMP in one of either solvents, solutions of decreasing concentrations were prepared, which would be later injected into the system in aliquots of 1 µL.

An example of the general behavior of the system is found at Fig. 12, right, where as a result of the dilution, the signal is far smaller and its recovery time decreases. However, it also shows a tendency present in almost all DMMP assays: for repeated injections or supply of the same theoretical amount of DMMP, be it on gas or liquid phase, there is an increasing tendency of the area corresponding to that injection. This was not only a direct consequence of the irreproducible manual injection of DMMP into the system, as there are other clear examples (Fig. 13) where this fact influences the repeatability of an assay. This fact leads to believe that DMMP could be slowly

accumulating in some zones of the pipe system over time, using the carrier gas as an agent to disperse itself, even though the system is kept at temperatures above 140ºC by heating tapes to prevent this effect.

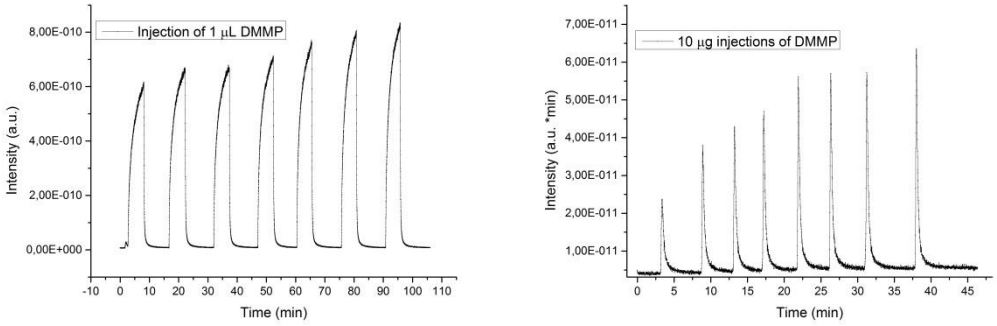

Fig. 12 Response of MS to: 1 µL of pure liquid DMMP (left) and repeated injections of 1 µL from a 10 mg/mL of DMMP in chloroform solution (right).

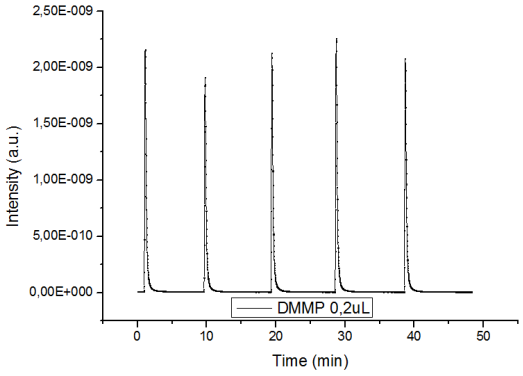

Fig. 13 Example showing the variation of peak response for the same theoretical injections.

One explanation addressed at the lack of reproducibility of the injections was, as cited before, the nature of manual injection, while another concerning issue was the difficulty to obtain a clear gas sample starting from liquid, as the liquid would have to vaporize in situ when injecting it to the pipe line. All of which is troublesome considering its high boiling point and the incapability to attain that temperature throughout the system.

Given the results up until this point, it seemed clear that liquid injection method was not viable to calibrate the system. Instead, the shift to calibration in gas phase deemed appropriate, as the irreproducibility due to the vaporization of the liquids would not be present.

In order to prepare the samples, several sealed bags of 10 L provided by Supelco were filled in with nitrogen at a rate of approximately 1 L/min for 10 minutes and different quantities of liquid DMMP were injected in each of them. The amount of

DMMP introduced in each bag was calculated to be well below the corresponding to the saturation of the compound at room temperature, calculated by Antoine's law. The increase in injected volume of material into the system was considerable, as the only reliable gas syringe at disposal was of 25 mL. In addition, as the liquid DMMP had to be vaporized, the sampling of the bag was performed the day next to its filling. Taking these parameters into account, a first set of experiments introducing mass of DMMP to the MS detector ranging from approximately 15 to 55 µg was performed. The experimental calibration curve is plotted in Fig. 14**¡Error! No se encuentra el origen de la referencia.**.

It is worth noting that for the calculation of the areas below each curve's pulses, the raw DMMP signal curve data was divided between the N_2 signal (28 uma) to counterbalance the pressure variation in the vacuum chamber , thus affecting the absolute values of either curves. In addition, due to the high noise affecting the low concentration samples, a smoothing of the curve in groups of 10 points by the Savitzky-Golay method was performed, whose comparison with the prime curve can be visualized at Fig. 14, right.

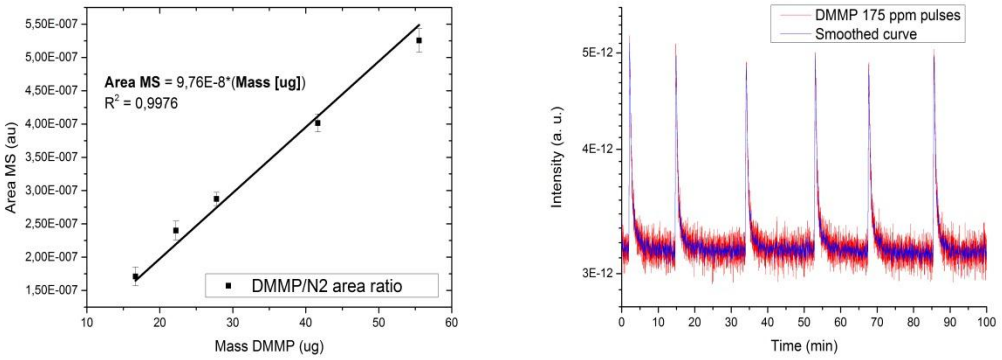

Fig. 14 Gas phase calibration curve of DMMP (left); application of the smoothing (right).

After obtaining a valid calibration curve, gas sampling cylinders were filled in with the N2-DMMP mixture obtained after passing a dry N2 stream through two DMMP saturators in series at temperature of 5 and 10 ºC. The main purpose of the experiment was to evaluate the concentration of the as prepared N2-DMMP mixture from the calibration factor previously obtained. Unlike the gas bags, the gas cylinders were left for 1 hour to achieve their homogenization with the gas flowing through it. Afterwards, the valves were closed and its content was directly injected to the MS. The treatment of the data was done similarly as in the case of the bags, with the difference that the basis for the calculation of the injected mass was that the saturation in DMMP

of the gas mixture leaving the saturators train was of 100% at the temperature of the thermostatic bath. The comparison of both calibration curves was plotted at Fig. 16, where a considerable difference between the slopes of the curves stands out. Some of the suggested causes that could have produced this disparity in data are:

- A possible positive gradient of temperature between the oil bath of the saturators and its content, yielding saturation at higher temperature that of expected and thus registering increasing mass of DMMP in the case of the saturators.
- A degradation of the DMMP in between the filling of the bags and its sampling or its adsorption in the walls of the bag or the sealing septum, which would be possible due to the preferential affinity of DMMP over the plastic rather than the glass of the cylinders. In the end, lower concentration in the gas phase would organic decrease the real concentration of the bags.
- A loss of DMMP liquid in the walls of the syringe that introduced it into the bags, lowering its maximum potential concentration.
- An incomplete filling of the 10 L gas bags or its eventual deflation could also meddle with the concentrations of DMMP introduced.

Considering that the adsorption performance will be evaluated using DMMP mixtures prepared from the saturator´s train, saturators, the applied calibration factor will be the following, where A is the peak area of the MS signal expressed as ratio of $I_{94\ uma}/I_{28\ uma}$:

$$\boldsymbol{Area\ MS = 3.73E - 8 \cdot Mass[\mu g]}$$

2.4.5 Analytical comparison of hexane and DMMP via MS

After installing the setup of Fig. 8 and executing the experiment conditions detailed at 2.4.3, the collected data was plotted at Fig. 15. The data collected at Fig. 14 will serve as comparison basis for the DMMP.

There are plenty of differences between the behavior of both gases: the recovery time is far shorter for the hexane (1-1.5 min for hexane vs an average of 10 for DMMP); the intensity of the signal is visibly superior in the case of hexane because although the ppmV in both cases are of the same order, hexane still yields a signal of E-10 order with a 1.8 mL while DMMP yields of E-12 after injecting 25 mL. As a consequence of this, the electronic noise contribution is far heavier in the case of DMMP and its limit of detection is of much higher value. In addition, there is a “memory” effect when working with DMMP and not with hexane: successive pulses of the same amount of gas results

in increasing areas of the peaks, which clearly shows at Fig. 12 and throughout all the DMMP experiments in general. In addition to all this, DMMP requires an installation heat insulated at a relatively high temperature (around 140 ºC) in order to avoid its adsorption within the transfer lines.

All in all, the character of DMMP heavily difficults the proper detection and monitoring of the substance within the proposed analytical system, which is bound to derivate into sensing complications when performing the adsorption experiments.

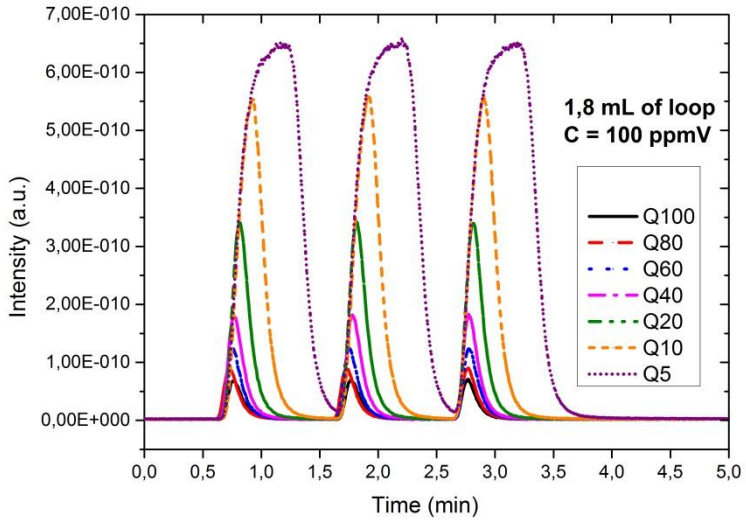

Fig. 15 Hexane signal for 3 loop pulses depending of the carrier gas flux at 100 ppmV.

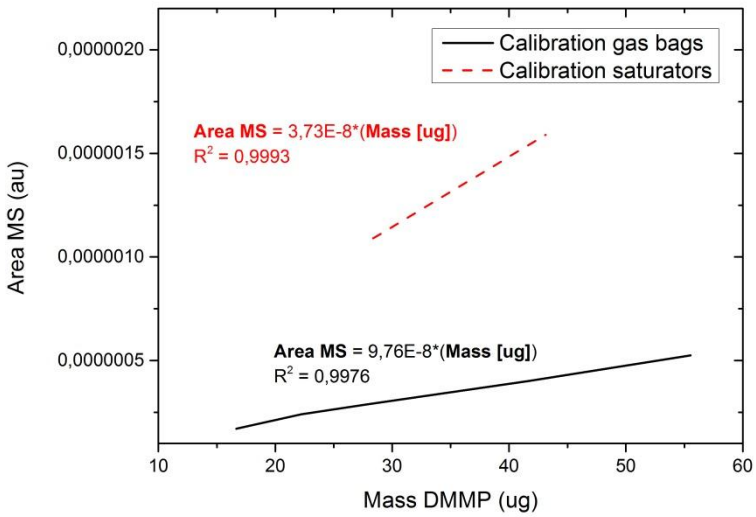

Fig. 16 Comparison of the DMMP calibration curves.

2.5 Physico-chemical Characterization Techniques

- X-ray Diffraction (XRD): The radiation was set to maintain its volumetric penetration constant, and its degree range was between 5 and 60 deg.
- Scanning electron microscopy (SEM): The microscope employed to take the pictures was the model SEM Quanta FEG 250, and the range of magnetic augmentations was generally between 1200 and 10000.
- Thermogravimetry analysis (TGA): A Q5000 SA was employed in the thermogravimetries using a N_2 atmosphere. In regards to the analysis performed for the MOF batches appearing in Fig. 19, the temperature range applied in the first case was of 20 to 600 ºC and of 20 to 900 ºC in the second, both with a heating rate of 5 ºC/min.
- Physisorption: The measurements were carried out at an ASAP-2020 equipment, using N_2 at 77 K as adsorbate in all cases. The load of MOF surpassed the 100 mg in all cases and the standard degasification conditions were the following:
  - Evacuation phase (30 min): Temperature increased at 10 ºC/min until 90 ºC and pressure at 0.67 kPa/s until a maximum of 9 kPa.
  - Heating phase (8 h): Heating rate of 10 ºC/min until 350 C.

3 Results

3.1 Zn precursor by Sublimation of Zinc Acetate

This procedure was deemed important in [5], where it is stated that the sublimated species (or zinc cluster) yields crystalline films, unlike the non-altered one. In order to assay the stability of the zinc cluster, several XRD analyses depending of the age of the product were performed (Fig. 17). It was observed that after several weeks of the synthesis, new diffraction peaks appear (which have been circled in the image), which could indicate the oxidation/rehydration of the sublimated material as well as the fact that the crystallization degree of the material is retained for a minimum of 10 days after production.

The same work [5], compared the performance of both types of acetates, and it concluded that in order to promote the formation of the right MOF structure, the degradation of the sublimated species is needed. The visual key for this phenomenon was that when initially dissolving the sublimated acetate the solution was transparent, and it would eventually turn into a white turbid suspension. This was not the case for

the commercial Zinc Acetate, as it would yield a whitish solution right upon dilution. Thus, any batch of the product which had not been sublimated in the previous 10 days was treated as if it were of commercial quality, not employing it in the MOF synthesis nor in the LbL procedure.

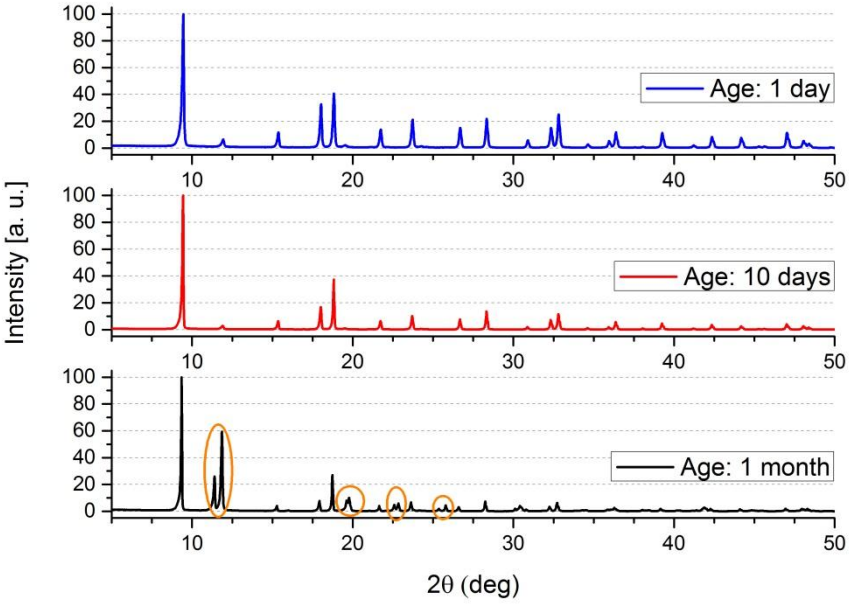

Fig. 17 Stability of the basic Zn acetate upon exposure to room conditions: XRD analysis.

3.2 Zn-DMCAPZ in powder form

As stated previously, this MOF-5 analogue was selected due to its supposed high hydrophobicity, thermal resistance (up to 400 ºC),specific surface area, i.e.up to 900 m^2/g and its median pore width circa 5.3 Å [5]. Herein, an extensive physico-chemical characterization was carried out to confirm these values. The different characterization techniques were generally applied to 2 batches of MOF, with the exception of physisorption, where a third batch was tested for the sake of reproducibility, as it is the only analysis that yields considerable differences amidst batches of product.

The normalized XRD data from the different MOF batches were compared to published data, denoted as A-MOF for the sake of convenience, to establish the possible similarities (Fig. 18). In general, the number and position of the main diffraction peaks are quite similar in all the cases, supporting the reproducible synthesis of MOF-5 type material.

The water uptake properties and thermal stability of the as synthesized MOF-5 type material, taken at room temperature, were evaluated by TGA and its results plotted

at Fig. 19. It was found that the synthetized MOF withstood temperatures above 400 ºC; as there was a mere loss of weight of around 5 % at 450 ºC. In addition, it was confirmed its high hydrophobic character, as there was a decrease of mass of less than 3 % in the low temperature region, i.e. 20-100 ºC in both cases. It is also worth noting the great stability of the compound, as the time span of approximately 6 months between the synthesis of the first batch and its TGA did not substantially alter the results in comparison to the second batch, even more so when the MOF samples were stored in a phial during all that period.

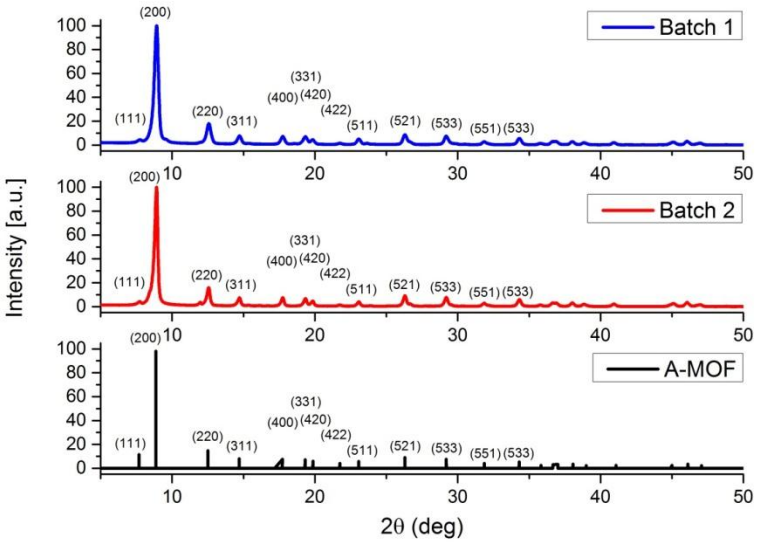

Fig. 18 XRD spectra comparison, "A-MOF" curve data taken from ***[5]****.*

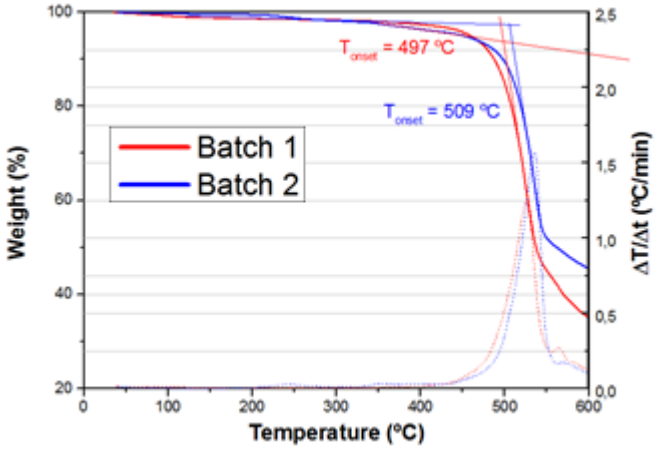

Fig. 19 TGA for 2 batches of Zn-DMCAPZ.

Textural properties of MOF-5 type materials were evaluated from N2 physisorption measurements. BET isotherm was used to calculate the specific surface area, and DFT theory to deduce the pore size and volume. The methodology applied to

the BET and DFT analysis were extracted from [8] and [9]. The summary of the calculations for the 3 batches analyzed is shown in Table 1.

The most outstanding feature of the analysis is the vastly superior BET specific area of the material (around 1500 m^2/g)when comparing with the highest reported for this MOF-5 analogue, i.e.900 m^2/g [5]. In the referenced work, the value of pore size (approximately 5.3 Å) is derived from adsorption experiments performed onto the material using adsorbates with different kinetic diameters. In the case of the herein synthetized MOF, the estimation of this parameter by the density functional theory (DFT) model was in the range of 5.3 Å, matching the pore size reported value.

Table 1 Summary of the textural properties for the as synthesized MOF-5 samples.

Batch	Batch 1	Batch 2	Batch 3	**Mean values**
BET area (m2/g)	1655	1388	1545	**1529 ± 134**
DFT median pore width (Å)	5.40	5.22	5.33	**5.32 ± 0.09**
DFT pore volume (cm3/g)	0.83	0.61	0.77	**0.74 ± 0.11**

Accounting from the XRD and TGA analyses, it is confirmed the formation of the right structure of Zn-DMCAPZ. The differences in BET values can be attributed to the dissimilarities of sample degasification procedures.

Fig. 20 shows SEM image of the synthesized powder. The majority of the crystals are cubic in shape with an average size around 100 nm. Crystals bigger than 200 nm were also found but were not included in the calculus of crystals size distribution due to its scarcity

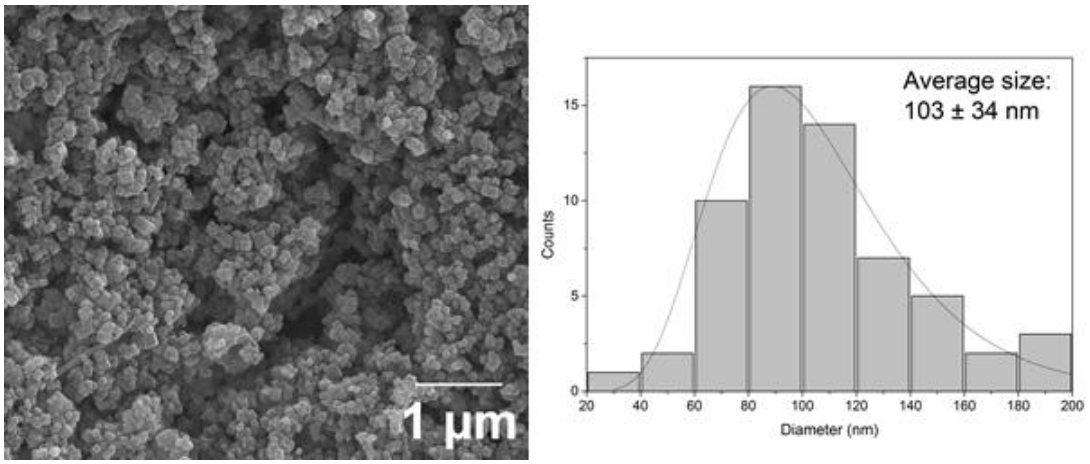

Fig. 20 SEM images of Zn-DMCAPZ powder and its corresponding histogram obtained by ImageJ analysis.

3.3 In situ growth of Zn-DMCAPZ layers

The general conditions for the LbL process on Pyrex plates were adapted from the previous work [5]. However, there were some conditions not well specified which led to irreproducible results and/or heterogeneous coatings. Among those, the oxygen plasma step and the constituent material of the reactor reveal crucial. In addition, the setup for the process involved plenty of manual handling unlike the one present in the reference, which employs a "washing machine" to automatize the LbL cycles. Thus, the process explained in this work could be clearly improved by means of appropriate instrumentation.

3.3.1 Influence of the plasma treatment

As stated in 2.3, two set of conditions ("*Plasma 1*" and "*Plasma 2*") were tested to treat the substrates, as well as not applying the procedure. The treatment fulfilled a double function: to clean further the surface from all possible organic residues and to hydrophilice the surface to promote the bond of the MHDA and, thus, of the MOF-5 analogue. The contrast between the effects of one method or another was visualized via SEM imaging.

The improvement in the cleaning of the surface is quite visible at (Fig. 21), where the left and the right pictures correspond to substrates with and without plasma treatment, respectively. Apart from the superior crystal growth of the "Plasma 2" sample, the surface of the second substrate is far dirtier (formation of multiple aggregates) and their crystals have a broader distribution of sizes. The number of LbL growth cycles was the same for 30 for both cases and the interphase portrayed in all the pictures is Pyrex-gold: left-right.

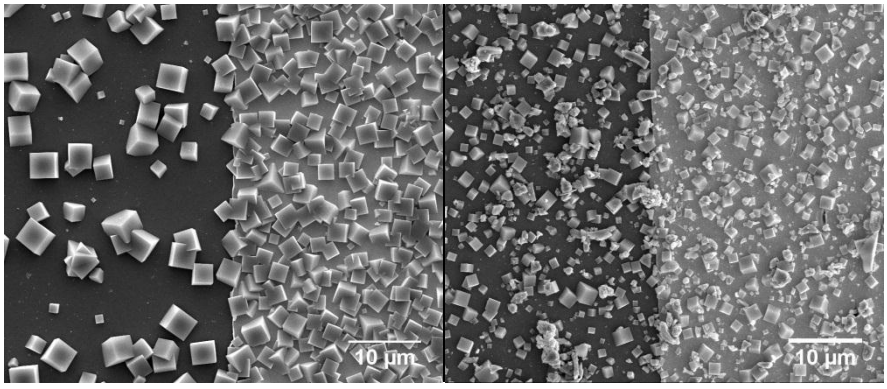

Fig. 21 Contrast of "Plasma 2" conditions (left) and no plasma (right).

The difference in the morphology of the sample between performing "Plasma 1" and "Plasma 2" can be observed at (Fig. 22). Setting aside the shift in the diameter of

the crystals, it is clear that the MOF has grown preferentially over the gold surface of the substrate, which could be related to the stage of surface activation by MHDA. As the plasma conditions for "Plasma 2" are more aggressive, it allows for a much higher hydrophillization of the surface. Given this instance, it is natural for MHDA to link preferentially to the gold its thiol bond is more energetically favorable than the hydroxyl bond that the agent could establish with the Pyrex.

3.3.2 Influence of reactor recipient

The first batch of MOF grown Pyrex substrates was performed inside 100 mL glass beaker reactors and it was observed that the volume of the solution decreased around 20 mL in the span of time of 5 cycles of LbL, as the solvent was mainly ethanol within a 50 ºC oil bath. Due to this, the next iterations of the process were moved into 120 mL plastic bottles as they could be sealed by a lid to avoid the evaporation.

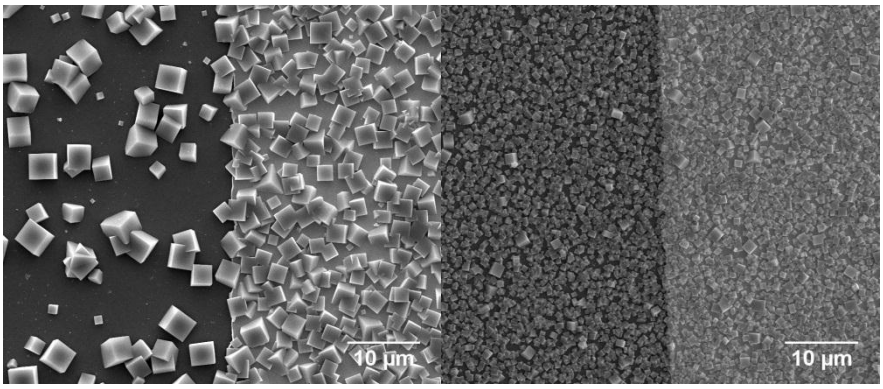

Fig. 22 Contrast of "Plasma 2" conditions (left) and "Plasma 1" conditions (right).

However, these processes proved unsuccessful in terms of growth of MOF and successive attempts altering the proportions of reactants and solvents were made in search for the optimal condition until the [10] work was discovered. The author also implemented the growth of another MOF material by a similar LbL method, and she discovered that by using a plastic container the growth was also occurring at the walls of the reactor, competing with the substrate. Following this event, the subsequent LbL reactions were to be carried out in the first used glass reactors. In (Fig. 23) it can be observed the contrast in using either reactor. Even when 10 more cycles have been completed for the substrate grown within a plastic beaker, the stage of growth corresponding to the glass beaker is visibly superior. Thus, glass containers were the appropriate choice to promote the reaction.

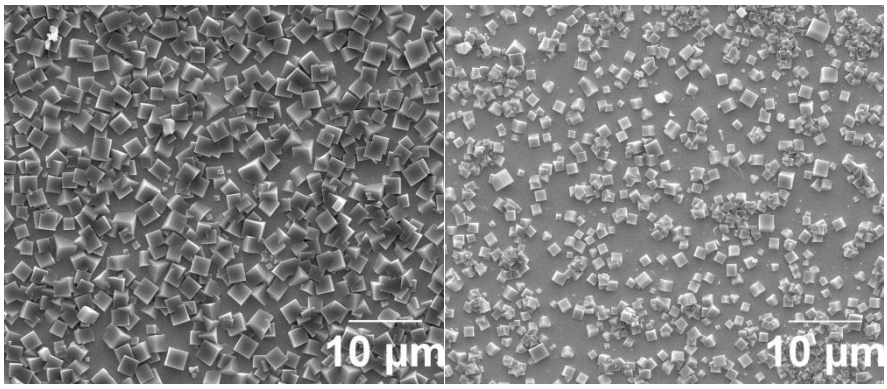

Fig. 23 Images of substrates with 30 LbL cycles grown using glass beaker (left) and 40 LbL cycles grown using plastic beaker (right).

3.3.3 Influence of the number of LbL cycles

The number of LbL cycles o performed on the µPC devoted to DMMP adsorption was 30, the plasma treatment employed was that of "*Plasma 2*" conditions and the reactions took place within a glass beaker. However, substrates with less number of repetitions were also studied by XRD and SEM to establish the correlation between crystal growth and number of reaction cycles.

Fig. 24 shows a compilation of images of the gold area of the substrates with 5, 10, 20 and 30 LbL cycles, respectively. While the size of the crystals grown on the plates does not vary substantially, their density does, reaching its maximum at 30 layers as it was expected. Because of this fact, measuring the height of the whole coating by visualizing the side face of the substrate had a degree of uncertainty. Table 2 shows the average crystal size for each case along with the estimation of the height of the layer (calculated from Fig. 25.b).

Lastly, Fig. 25.shows the interface between the Pyrex and the Cr/Au electrodes patterned on the surface. It is interesting to note the preferential growth of Zn-DMCAPZ over the gold in terms of density (understood as number of crystals per unit of area) thanks to the SAM layer deployed on it. The stronger interaction between the MHDA and the gold during the incubation stage is attributed to the S-Au covalent interactions. Thus, the inclusion of the incubation step in the activation of the plates is highly recommended.

Due to this effect, the usual step for sealing the microdevice by Si-Pyrex anodic bonding was impossible, as it requires a completely smooth surface all throughout the Pyrex. Taking this into consideration, the sealing by application of Acc Silicoset 158 was mainly used.

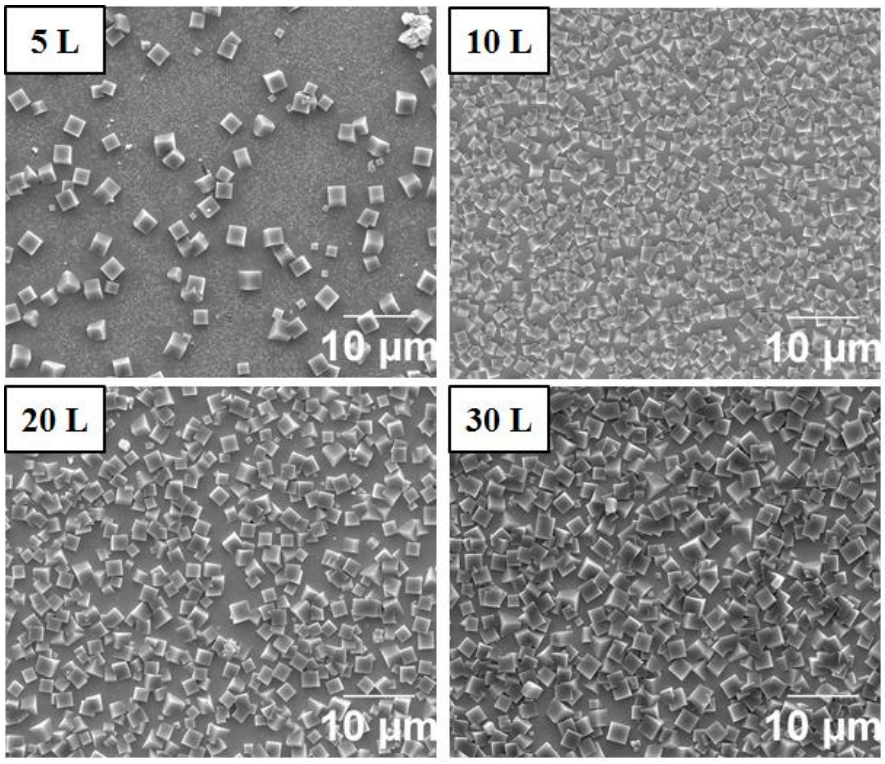

Fig. 24 SEM images of the MOF layer on micropreconcentrators as a function of the number of LbL cycles or "L".

Table 2 Crystal Size and Layer thickness values derived from SEM analyses.

Sample	5 Layers	10 Layers	20 Layers	30 Layers
Diameter (µm)	1.8 ± 0.3	1.2 ± 0.2	1.8 ± 0.4	2.0 ± 0.3
Height (µm)		0.8 ± 0.1		

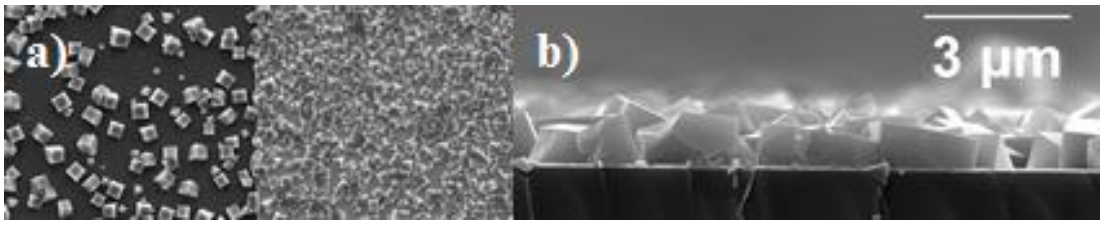

Fig. 25 SEM images for a) Pyrex (left) – Gold (right) interphaseand; b) Cross-section of the obtained layers after for 30 cycles of LbL growing.

SEM observations revealed that an increase of the LbL cycles yielded coatings of higher MOF density. To support this observation, XRD analyses were also performed for each of the samples studied. (Fig. 26) presents a comparison of MOF-5 layers prepared by 35 LbL cycles on silica support (adapted from [5]), the resulting layer herein obtained on Au coated Pyrex after 30 LbL cycles and the MOF-5 in powder form. All the XRD spectra are normalized to the main MOF-5 characteristic diffraction peak at $2\Theta=8.9^{o}$. Some minor differences in relative intensities distribution can be

observed due to preferential orientation effects. The crystallinity and crystal density evolution with number of LbL cycles has been monitored by the intensity values of the main MOF-5 diffraction peak. A linear fitting between number of LbL cycles and the ratio $\frac{\text{Area of MOF's main diffraction peak (8.9 deg)}}{\text{Area of Pyrex's main diffraction peak (38.3 deg)}}$ was obtained. This behavior confirms the clear correlation between these 2 parameters, see Fig. 27. As the regression coefficient is close to 1, the aforementioned hypothesis was confirmed.

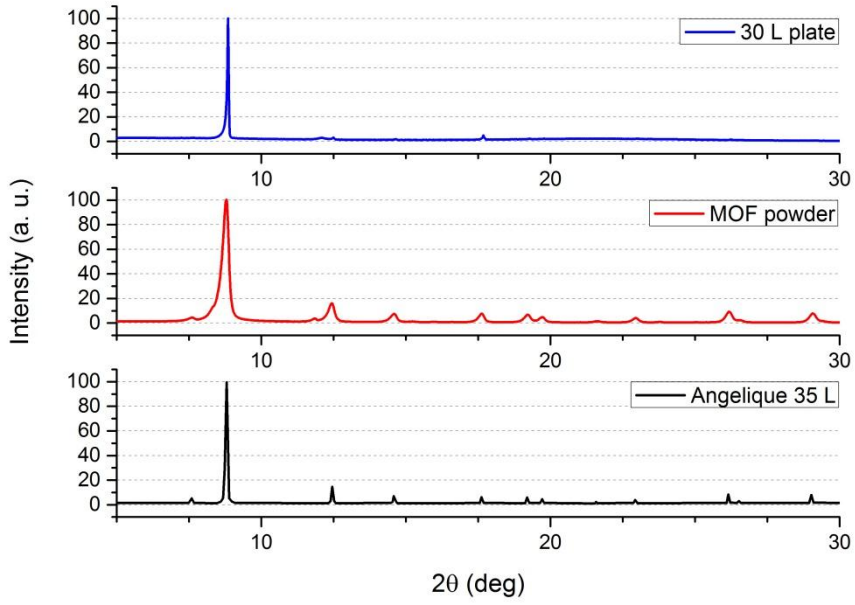

Fig. 26 XRD spectra comparison of MOF-5 layers prepared by LbL

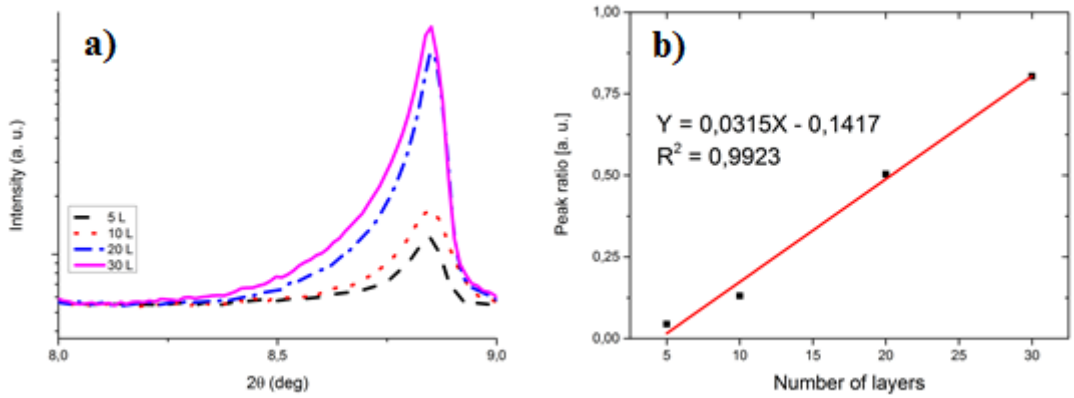

Fig. 27 Study of crystal density evolution with number of LbL cycles by XRD: a) analysis of the main MOF-5 diffraction peak; b) linear dependence of XRD counts with number of cycles,

3.4 **DMMP adsorption experiments**

After setting up the plant as according to (insert reference to scheme adapted from from

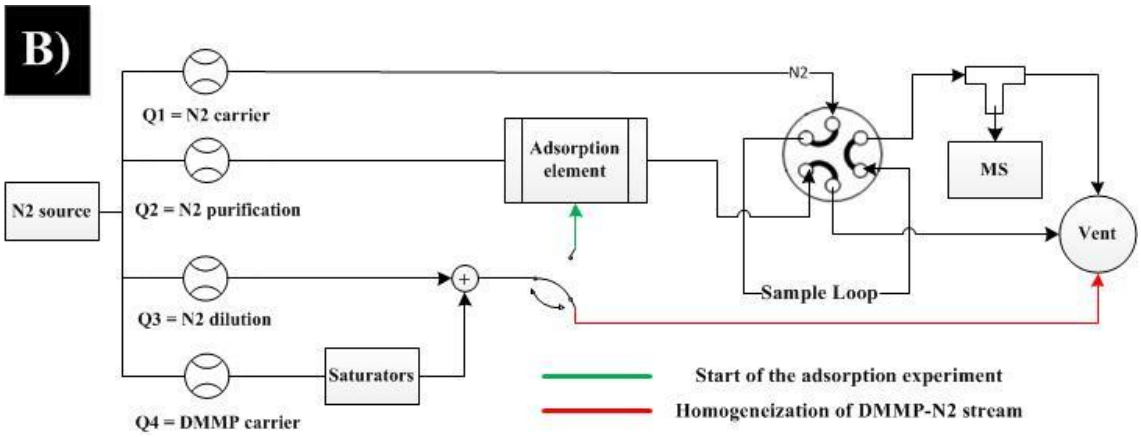

Fig. 10) the adsorption performance for both a fixed bed reactor filled with Zn-DMCAPZ powder and a µPC composed of a 30 LbL cycles grown pyrex plate was evaluated. The objectives were: to obtain the breakthrough curve, to evaluate the sorption efficiency and to estimate the total amount of DMMP adsorbed.

As a means of sample degassification, a dry nitrogen stream(80 or 10 mL/min for either the fixed bed reactor or the µPC, respectively) was supplied to the reactor while the heating tapes were switched on, all during the night prior to the experiment. At the same time, the stream of N_2-DMMP flowed through the saturators, whose oil bath temperature was set to 35 ºC, until the vent, for the sake of its homogenization.

3.4.1 Fixed bed reactor

A cubic cylinder of porous stainless steel approximately 5 mm of diameter and 10 mm of height was loaded with 28.9 mg of Zn-DMCAPZ (Batch 2) for the experiment. The stream of N_2-DMMP mixture supplied to the reactor was 795 ppm of DMMP with a total flux of 80 mL/min (30:50 mL/min DMMP:N_2), which crossed the reactor in radial flow regime.

The calculations were carried out as described in 2.4.2 and its results were reflected at Fig. 28. The normalization of the curve to the maximum concentration was done using said sample's maximum signal in order to approximate the sorption efficiency of the material (Fig. 29). The maximum adsorption was considered completed at around 70 min and, in order to calculate the adsorption parameters, a Boltzmann fit using the Levenberg Marquadt was performed to both the raw and the normalized data. The delay time between the time mark of 0 minutes and the actual

response of the system to an stimuli was of 0.5 minutes and as such was set as the initial time for all the calculations.

Following the instructions exposed at 2.4.2, the targeted adsorption parameters were calculated and represented at Table 3 along with the data related to the µPC.

3.4.2 Micropreconcentrator

The Zn-DMCAPZ grown micropreconcentrator portrayed in (insert imagen preconcentrador) was connected to the transfer lines replacing the position of the bed reactor. Due to the maximum pressure limitations of the sealing of the µPC, the inlet stream was 10 mL/min of pure DMMP, which stands for a concentration of 2120 ppm.

It is worth mentioning that as the mass of the Pyrex substrate was not measured prior to the growing cycles, the real mass of MOF crystals over the µPC is unknown. Knowing the average height of the layer was of 0.8 µm (Table 2), the surface area of the gold grown over the Pyrex (69 mm^2) would yield the volume of MOF. According to the reported values of MOF-5 density, its value ranges from 0.64 to 2.03 g/cm^3 [11].

In this experience, the saturation of the material appeared to be achieved around the 100 min lapse, whose correspondent intensity was taken as basis to normalize the curve. The treatment of the data was parallel to what was done in the case of the fixed bed reactor. The representation of the raw and normalized curves are found at Fig. 28 and Fig. 29, respectively, and the summary of the calculations at Table 3.

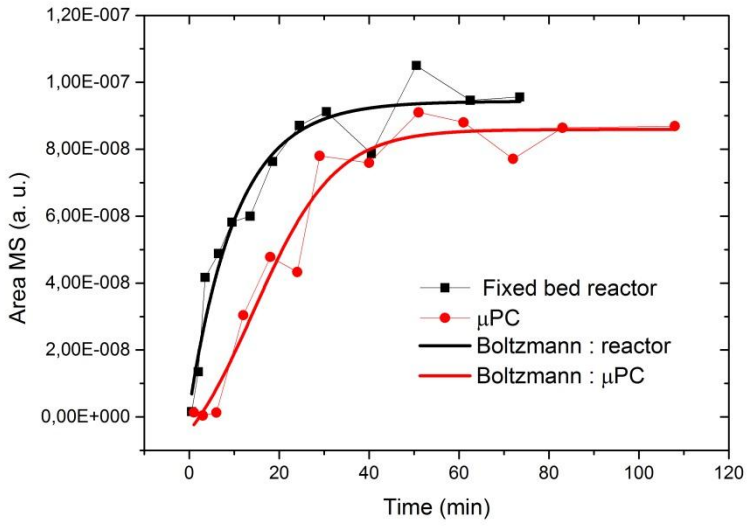

Fig. 28 Kinetic adsorption experiments for both the fixed bed reactor and the µPC.

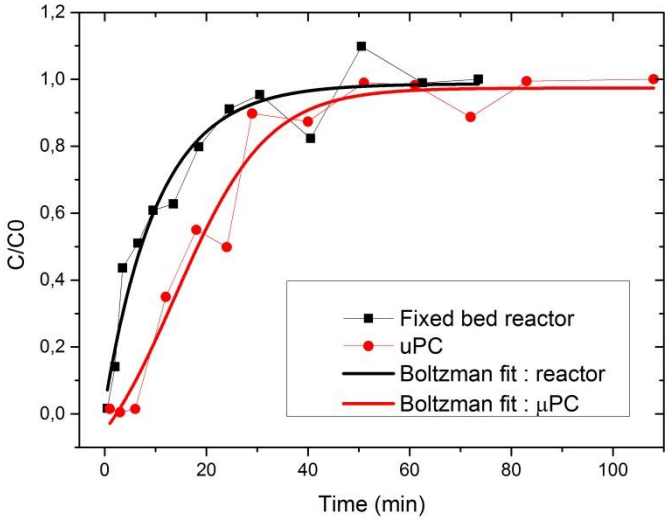

Fig. 29 Kinetic adsorption experiments normalized to their maximum concentration.

Table 3 Summary of the adsorption experiments.

Sample	Mass of MOF (mg)	Adsorbed DMMP mass (ug)	Maximum adsorbed DMMP at 30 ºC (ug)
Fixed bed reactor	29	24	4074
µPC	Non available*	45	Non available*
Sample	**Sorption efficiency**	**$t_{0.1}$ (min)**	**$t_{0.95}$ (min)**
Fixed bed reactor	0.036	0.8	31
µPC	0.285	6.0	43

*Due to the lack of the value of the layer's weight.

3.4.3 Evaluation of the adsorption parameters

Previous works in the NFP research group towards the characterization of micropreconcentrators, as [6], found values of sorption efficiency around 0.9 in the case of a micropreconcentrator and 0.471 in the case of a fix-bed reactor filled in with the same sensing material, i. e. silicalite-1. In this work, however, the efficiencies are far below to what was expected. This fact is probably due to an inefficient solid packaging in the fixed bed reactor configuration.

In the case of the µPC, the sorption efficiency is higher although lower than expected probably due to the analytical limitations. Blank assays on both configurations, without MOF are in progress to corroborate these preliminary results.

4 Conclusions

Within this work, the synthesis and characterization of the promising MOF-5 variant Zn-DMCAPZ, both in bulk powder and grown over Pyrex based substrates for its subsequent integration in the silicon based micropreconcentrators for the adsorption of the Sarin gas analogue.

By means of various characterization techniques, the properties of the MOF in question proved superior in contrast with works of other authors, as the synthetized material exceeded by 600 m^2/g the maximum reported specific area (900 m^2/g).

Using the layer by layer growth procedure, a thin and homogeneous coating of the MOF was applied to gold evaporated Pyrex substrates, which were successfully bonded to its silicon counterpart forming the micropreconcentrator.

Regarding the study of DMMP adsorption, an isotherm at 30 ºC describing its thermodynamical equilibrium with the MOF in question was successfully calculated, up to 15% in weight when exposed to saturated conditions at 30ºC.

As a side conclusion of the experiences of DMMP sensing via MS, the gas was deemed highly complicated to work with due to its low sensitivity, long recovery times, large tendency to adsorb throughout the transfer lines and "memory effect" among other factors, thus discarding its feasible and consistent analysis in the current system.

5 References

[1] K. Ganesan, S. K. Raza, and R.Vijayaraghavan, "Chemical warfare agents," *J Pharm Bioallied Sci.*, vol. 2, no. 3, pp. 166–178, 2010.

[2] R. Yoo, S. Cho, M. J. Song, and W. Lee, "Highly sensitive gas sensor based on Al-doped ZnO nanoparticles for detection of dimethyl methylphosphonate as a chemical warfare agent simulant," *Sensors Actuators, B Chem.*, vol. 221, pp. 217–223, 2015.

[3] F. Almazán *et al.*, "Zeolite Based Microconcentrators for Trace-Level : Fabrication and Performance," *J. Micromechanics Microengineering*, vol. 26, no. 8, pp. 1–18, 2016.

[4] F. Almazán *et al.*, "Design of a Microfluidic Device for Chemical Warfare Agents Adsorption using MOF-type Materials." Poster presented at XXXVI Reunión Bienal de la Real Sociedad Española de Química (RSEQ) - 2017

[5] A. Bétard, "Growth and chemistry of metal-organic framework thin films: torward functional coatings," *Dissertation*, 2011.

[6] F. Almazán *et al.*, "Zeolite based microconcentrators for volatile organic compounds sensing at trace-level: fabrication and performance," *J. Micromechanics Microengineering*, vol. 26, no. 8, p. 84010, 2016.

[7] J. Bryant-Genevier and E. T. Zellers, "Toward a microfabricated preconcentrator-focuser for a wearable micro-scale gas chromatograph," *J. Chromatogr. A*, vol. 1422, pp. 299–309, 2015.

[8] J. Rouquerol, P. Llewellyn, and F. Rouquerol, "Is the bet equation applicable to microporous adsorbents?," pp. 49–56, 2007.

[9] P. I. Ravikovitch and A. V. Neimark, "Density functional theory of adsorption in spherical cavities and pore size characterization of templated nanoporous silicas with cubic and three-dimensional hexagonal structures," *Langmuir*, vol. 18, no. 5, pp. 1550–1560, 2002.

[10] C. M. Karman, "3D structuration of MOF layers for gas sensors enhancement and its application in microreactors," 2014.

[11] J. J. Purewal *et al.*, "Increased volumetric hydrogen uptake of MOF-5 by powder densification," *Int. J. Hydrogen Energy*, vol. 37, no. 3, pp. 2723–2727, 2012.